Journal of Engineering Mathematics (2006) 54: 159–180
DOI 10.1007/s10665-005-9019-9

Joule-heating effects in mixed electro-osmotic and pressure-driven microflows under constant wall heat flux

KEISUKE HORIUCHI, PRASHANTA DUTTA* and AKRAM HOSSAIN[1]
Mechanical and Materials Engineering, Washington State University, Pullman, WA 99164-2920, USA
E-mail: dutta@mail.wsu.edu
[1]*Civil and Environmental Engineering, Washington State University, Richland, WA, USA*

Received 23 June 2004; accepted in revised form 30 August 2005 / Published online: 16 November 2005

Abstract. Heat-transfer characteristics of mixed electro-osmotic and pressure-driven flows are obtained in a two-dimensional straight microchannel by solving a steady-state energy equation. Both thermally developing and fully developed regions are considered for hydraulically fully developed mixed flows under isoflux channel wall conditions. The steady temperature distribution is obtained from the superposition of homogeneous solution and particular function. The particular solution is derived based on the constant heat-flux condition in the fully developed region, while the homogeneous solution is presented in terms of infinite series containing Kummer confluent hypergeometric functions due to the existence of non-self-adjoint eigenvalues. The coefficients of the homogeneous solution are found by utilizing the Gram-Schmidt orthogonalization procedure, and the Secant method is utilized to obtain the corresponding eigenvalues. Our analytical techniques are verified by obtaining an excellent agreement with existing literature for slug, pressure-driven, and pure electro-osmotic flow cases. In the fully developed region, the Nusselt number of mixed flow is independent of the thermal Peclet number for a particular Joule heating and imposed surface heat flux. The entry length of mixed flow significantly depends on the applied/induced pressure gradient to the electro-osmotic flow.

Key words: extended Graetz problem, Joule heating, microfluidics, mixed electro-osmotic and pressure-driven flows

1. Introduction

Microfluidics is one of the most rapidly growing fields in micro-electro-mechanical systems technology due to its applications in medical science, biology, and analytical chemistry [1–4]. Microchannels or capillaries are basic components of all microfluidic devices, and they have the potential of reducing the fabrication costs and consumption of chemicals as well as shortening the time of biochemical analysis. Over the last ten years, capillaries have been mainly used for capillary electrophoretic (CE) methods due to the high separation efficiencies and peak resolution. Microchannels have recently attracted the researchers' attention because they are less expensive, simpler and faster to fabricate complicated networks for "lab-on-a-chip" devices than capillaries.

In order to transport and control fluids in microchannels, electrokinetic pumping is the most popular technique due to its ability of dispensing a wide (conductivity) range of working fluids [5]. Electro-osmosis, one of the most common electrokinetic phenomena, is the bulk motion of an ionized fluid with respect to a stationary charged surface under the action of an external electric field [6, Section 6.4]. In recent years, a number of research groups have demonstrated electro-osmotic microflows in various shaped microstructures [7, 8]. Electro-osmotic

*Corresponding author.

flows mainly originate from the interaction between an electric double layer (EDL) and an externally applied electric field. This interaction of the electric field and the charged ions results in thermal energy generation such as Joule heating.

Joule heating can cause perturbation of the sample band during iso-electric focusing and loss of biological activity during biochemical assays due to thermal diffusion [9–12]. The experimental study by Burgi *et al.* led to the conclusion that, in CE, the internal temperature increases by 1·1° C for an thermal energy generation of 0·1 W [13]. In typical electro-osmotic flows with a fluid of 300 μS/m electrical conductivity and an applied electric field of 10 V/mm, the Joule-heating term contributes 3×10^4 W/m^3. This thermal energy generation and associated dissipation mechanisms have received very little attention in research on microfluidic channels. Recently, Maynes and Webb studied the thermal behavior of the fully developed pure and mixed electro-osmotically driven micro-flows [14,15], but their analysis is not valid in the entrance region. The entrance region is very important in many electrophoretic separation processes, such as temperature-gradient focusing where a constant temperature gradient is required throughout the channel [16].

In this article, the Joule-heating effects of mixed electro-osmotic and pressure-driven microflows are analyzed in a two-dimensional straight microchannel under isoflux wall thermal conditions. Our study assumes a hydrodynamically fully developed behavior from the channel entry. However, in thermal analysis, both thermally developing and fully developed regions are considered. Analysis of the energy equation in the developing region is particularly challenging due to the presence of both inertial and viscous terms. Graetz solved the classical laminar convection heat-transfer problem in thermally developing regions for the parabolic velocity distribution under the isothermal wall condition [17]. This original Graetz problem was solved for circular pipe flows by neglecting both axial-conduction and heat-generation terms from the energy equation. Later on, a number of research groups have considered the contribution of the axial-conduction terms in the analytical treatment of energy equations when the Peclet number is less than 100 [18–23]. This particular problem is known as the extended Greatz problem. Solving the extended Graetz problem is mathematically challenging, since the associated eigenvalue problem is non-self-adjoint when compared to the standard Sturm-Liouville problem. Based on the extended Graetz problem, various kinds of flows, such as liquid metal flow in compact heat exchangers [24] and magnetohydrodynamic flows [25] have been analyzed. However, none of these previous studies have, until now, dealt with electro-osmotic flow in which the flow velocity distribution is different from pressure-driven flows. Moreover, none of the above analytical studies have considered the thermal-energy generation in the system due to volumetric Joule heating. In a seminal work, Sparrow and co-workers studied the effect of an arbitrary generation term in pressure-driven thermally developing flows, and they obtained analytical solutions for the heat-transfer characteristics [26]. Recently we presented the heat-transfer characteristics of pure electro-osmotic microflows in a two-dimensional straight channel with volumetric Joule heating [27]. However, in most electrokinetically driven microflows, mixed electro-osmotic and pressure-driven flows result instead of a pure electro-osmotic flow. In this analysis heat-transfer characteristics of mixed electro-osmotic and pressure-driven flows are obtained in both (thermally) developing and fully developed regions. This analysis considers the interaction of the advection, diffusion, and Joule heating terms in order to obtain the temperature distribution of the fluid in microchannels. Due to the presence of the pressure-driven component of the velocity in the advection term, the energy equation is not separable for mixed flow cases.

Table 1. Nomenclature.

A_c	cross-sectional area of a microchannel
A_n	coefficients
B_n	coefficients
c_p	specific heat at constant pressure
D	half channel height
D_H	hydraulic diameter
$\vec{E}$	applied electric field
E_x	electric-field component in the streamwise direction
e	electron charge
f_n	eigenfunctions
G	normalized generation term, $\sigma(\vec{E}\cdot\vec{E})D/q_s''$
g_n	orthogonal functions
h	local heat-transfer coefficient
k	thermal conductivity
k_B	Boltzmann constant
n_o	average number of positive/ negative ions in the buffer
Nu_ξ	local Nusselt number
P	pressure
P^*	normalized pressure, $PD/\mu u_{HS}$
Pe_T	thermal Peclet number
Pr	Prandtl number
q_s''	surface heat flux
Re	Reynolds number based on Helmholtz-Smoluchowski velocity
R_{ev}	ratio of Joule heating to viscous dissipation
T	temperature
U	normalized streamwise velocity, u/u_{HS}
u	velocity component in the streamwise direction
u_{HS}	Helmholtz-Smoluchowski velocity
$\vec{V}$	velocity field
v	velocity component in the cross-stream direction
W	channel width
x	streamwise distance
y	cross-stream distance
z	valence

Greek letters

α_{ij}	constant, $\langle f_i, f_j\rangle/\|f_j\|^2$
ΔT	dimensional temperature difference, $T_s - T$
$\Delta\theta$	normalized temperature difference, $\theta_s - \theta$
ε	permitivity of the medium
Φ	viscous dissipation
η	normalized cross-stream distance, y/D
λ	Debye length
λ_n	eigenvalues
μ	dynamic viscosity
θ	normalized temperature, $(T - T_e)k/(Dq_s'')$
ρ_e	electric charge density
ρ_f	fluid density
σ	electrical conductivity of the buffer fluid
Ω	normalized pressure gradient, $-(1/2)(dP^*/d\xi)$
ξ	normalized streamwise distance, x/D
ψ	electrokinetic potential
ζ	zeta potential

Subscripts

c	centerline
e	inlet
fd	thermally fully developed region
g	general solution
m	mean
p	particular solution
s	surface

2. Mathematical treatment

2.1. Electric double layer

Most surfaces acquire a net electric charge when they come in contact with a polar medium via ionization, ion adsorption, or ion dissolution. For example, a glass surface immersed in water undergoes a chemical reaction in which a fraction of the surface silanol group SiOH are changed to SiO^- or $SiOH_2^+$, resulting in a net negative or positive surface potential depending on the pH of the solution [28]. This influences the distribution of the ions in the buffer solution as shown in Figure 1. Here the positive ions cluster right next to the negatively charged wall forming the Stern layer, a layer of typical thickness of a few ionic diameters. The ions within the Stern layer are attracted to the wall by very strong electrostatic forces ($10^7 \sim 10^9$ V/cm) [29]. Hence, ions in this layer are mostly immobilized. Right next to the Stern layer, thermal movement of ions plays an active role, and develops the diffuse layer that contains both co-ions and counter ions. Stern and diffuse layers form the EDL. The ion distribution within the diffuse layer is governed by the Poisson-Boltzmann equation, which is

$$\nabla^2 \psi = -\frac{\rho_e}{\varepsilon}, \tag{1}$$

where ψ is the electrokinetic potential, ε is the permittivity of the medium, and ρ_e is the electric-charge density (see Table 1). For a symmetric univalent electrolyte, the electric-charge density can be presented as [6, Section 6.4]

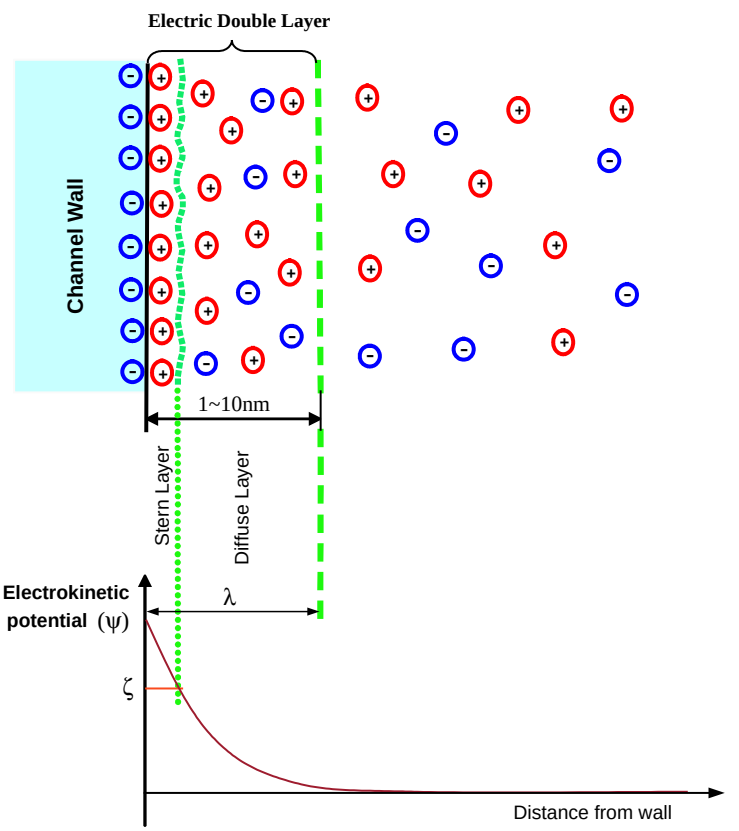

Figure 1. Electric double layer next to a negatively charged surface.

$$\rho_e = -2n_0 ez \sinh\left(\frac{ez\psi}{k_B T}\right), \tag{2}$$

where n_0 is the average number of positive or negative ions in the buffer, e is the electron charge, z is the valence, k_B is the Boltzmann constant, and T is the temperature.

Now consider a two-dimensional straight microchannel as depicted in Figure 2(a). In most microfluidic channels, the channel width is much larger than the channel height ($W >> 2D$). Although it is possible to fabricate microchannels of different aspect ratio ($W/2D$), a planar

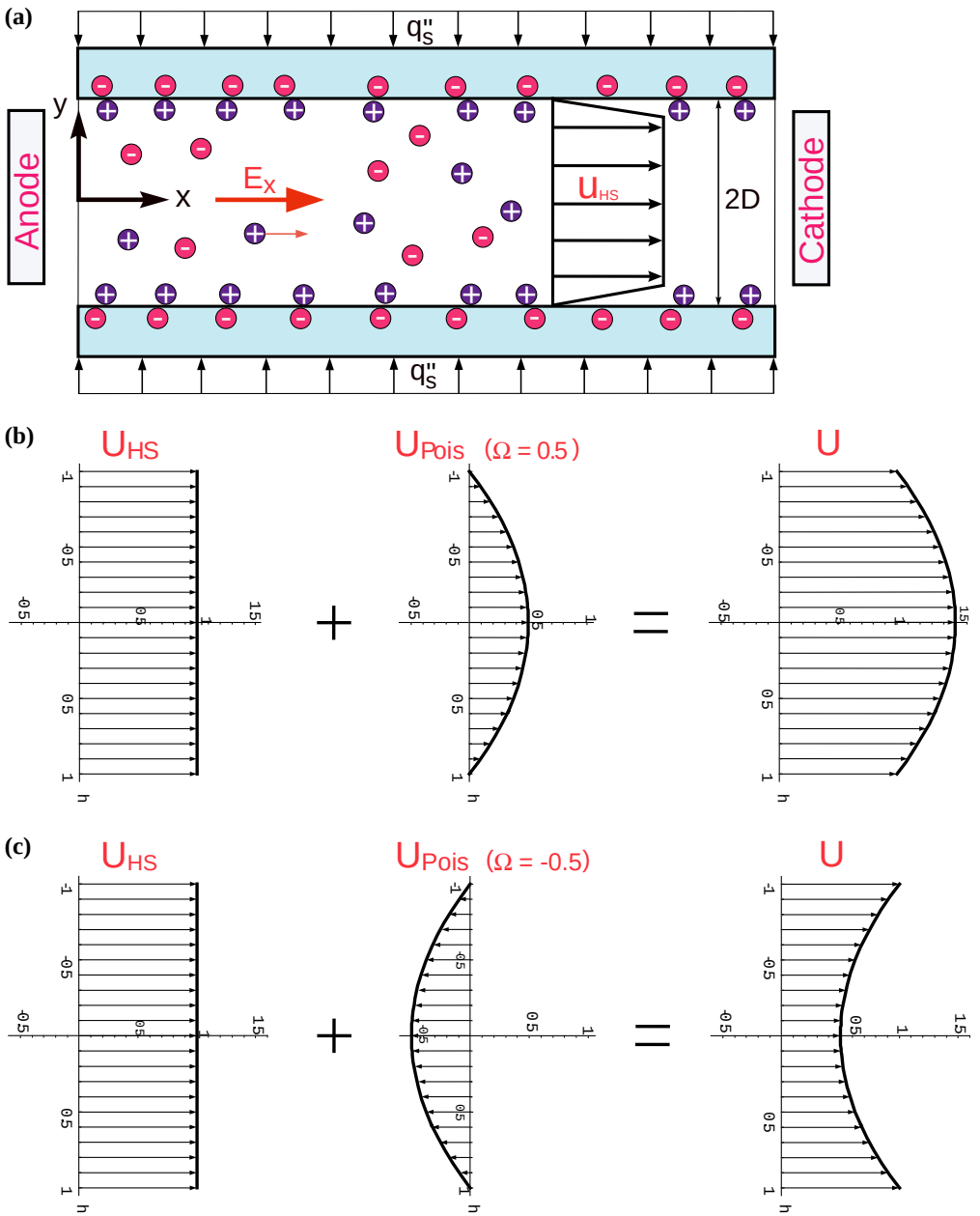

Figure 2. (a) Schematic view of electro-osmotic flow in a planar microchannel. Due to geometric, electrokinetic and thermal symmetry only upper half of the channel is analyzed for heat transfer characteristics. (b) Favorable-pressure-gradient mixed flow ($\Omega = 0{\cdot}5$) and (c) adverse-pressure-gradient mixed flow ($\Omega = -0{\cdot}5$).

channel is preferred from a diagnostic point of view [7]. For a planar channel, the variation of any variable in the width direction can be neglected. Therefore, in a two-dimensional microchannel, Equations (1) and (2) can be combined to obtain electrokinetic potential as [28]

$$\psi = \frac{4k_B T}{ez} \tanh^{-1}\left\{\tanh\left(\frac{ez\zeta}{4k_B T}\right)\exp\left[\frac{|y|-D}{\lambda}\right]\right\}, \tag{3}$$

where ζ is the zeta potential, y is the cross-stream coordinate system, and λ is the Debye length. The Debye length is an estimate of the EDL thickness, and it is a function of ion density (n_0). For aqueous solutions at 25°C, ion densities of 1 mM and 100 mM correspond to Debye lengths of 10 nm and 1 nm, respectively [6]. Typical ranges of electrokinetic, flow and thermal parameters are presented in Table 2.

2.2. Electro-osmotic flow

Figure 2(a) shows an electro-osmotic flow in a straight microchannel, where the channel walls contain net negative charges. In this particular case, the EDL has net positive charges. Therefore, the streamwise component of the externally applied electric field interacts with the EDL, and creates a net movement of positive ions in the downstream direction. The steady incompressible electro-osmotic flow is governed by the modified Navier-Stokes equations as follows [28]:

$$\rho_f(\vec{V}\cdot\nabla)\vec{V} - \mu\nabla^2\vec{V} + \nabla P - \rho_e\vec{E} = 0, \tag{4}$$

where ρ_f is the fluid density, P is the pressure, μ is the dynamic viscosity, $\vec{E} = (E_x, E_y)$ is the applied electric field, and $\vec{V} = (u, v)$ is the velocity field. The incompressibility of the working fluid is expressed by the continuity equation, $\nabla\cdot\vec{V} = 0$. The first and second terms of (4) show inertial and viscous forces, while the third and the fourth terms represent pressure and electrokinetic body forces, respectively. The main simplifying assumptions and approximations used in defining the flow equations are:

1. The fluid viscosity is independent of the shear rate. Hence, we assume a Newtonian fluid.
2. The fluid viscosity is independent of the local electric-field strength.
3. The ions are point charges and their convection effects are negligible. Hence, our analysis is valid for Stokes flows or for (hydraulically) fully developed channel flows.
4. The solvent is continuous and its permittivity is not affected by the overall and the local electric-field strength.

Table 2. Typical length scale, flow, and electrokinetic parameters considered in this theoretical work.

Parameter	Range
Half channel height, D (μm)	10–100
Electrolyte concentration, n_o (mM)	1–100
Debye length, λ (nm)	1–10
Characteristic length ratio, D/λ	1000–100,000
Axial electric field, E_x (V/mm)	10–500
Zeta potential, ζ (mV)	−100–100
Reynolds number, $\mathrm{Re} = u_{HS} D\rho_f/\mu$	0·002–0·700
Thermal Peclet number, $\mathrm{Pe_T} = \mathrm{RePr}$	0·01–5

5. Fluid properties are independent of temperature change. This can be justified for smaller temperature changes (less than 10K).
6. The zeta potential is uniform throughout the channel wall.

2.3. Analysis of mixed flows

Recent experimental results show that electro-osmotic velocities in microchannel are generally slow, having very low Reynolds number, $\mathrm{Re} < 1$. Therefore, the inertial term in (4) is negligible compared to the viscous term. In the case of pure electro-osmotic flow there is no pressure gradient, and the electrokinetic body-force term is counter-balanced by the viscous term. Thus, in a two-dimensional straight microchannel, the pure electro-osmotic velocity can be presented as [28]

$$u_{\mathrm{EOF}} = -\frac{\zeta \varepsilon E_x}{\mu}\left\{1 - \frac{\psi}{\zeta}\right\} = u_{\mathrm{HS}}\left\{1 - \frac{\psi}{\zeta}\right\}, \tag{5}$$

where $u_{\mathrm{HS}} = -(\zeta \varepsilon E_x)/\mu$ is the Helmholtz-Smoluchowski velocity.

Although electrokinetic flow is desired in many bio-analytical applications, there may be pressure variations along the channel for the following reasons:

- higher or lower electric-field strength at any particular location of the flow;
- presence of alternative pumping mechanism;
- placement of a mechanical valve in the flow path.

The resulting pressure gradient may distort the plug-like velocity distribution as shown in Figure 2(b) and (c). The velocity distribution in the mixed flow regions can be obtained from a linear superposition of electro-osmotic and pressure-driven flows [28]:

$$u(x, y) = u_{\mathrm{EOF}} + u_{\mathrm{Pois}} = u_{\mathrm{HS}}\left\{1 - \frac{\psi}{\zeta}\right\} - \frac{D^2}{2\mu}\frac{\mathrm{d}P}{\mathrm{d}x}\left\{1 - \left(\frac{y}{D}\right)^2\right\}, \tag{6}$$

where $u_{\mathrm{Pois}} = -D^2/(2\mu)(\mathrm{d}P/\mathrm{d}x)\{1 - (y/D)^2\}$ is the plane Poiseuille-flow velocity.

Equation (3) shows that the electrokinetic potential, ψ, decreases abruptly from the wall toward the center of the channel. For a two-dimensional straight microchannel, the electrokinetic potential diminishes within the effective EDL thickness, δ_{99}, ($\delta_{99}/D \leq 4\%$) [28]. Therefore, we neglect the effect of electrokinetic-potential distribution in the velocity distribution.

2.4. Energy transfer in the mixed flow

The governing equation for steady-state thermal-energy transport in mixed electro-osmotic and pressure-driven flows can be presented as

$$\rho_{\mathrm{f}} c_p(\vec{V} \cdot \nabla)T - \nabla \cdot (k \nabla T) - \Phi - \sigma(\vec{E} \cdot \vec{E}) = 0, \tag{7}$$

where c_p is the specific heat capacity, T is the temperature, k is the thermal conductivity, Φ is the viscous dissipation, and σ is the electrical conductivity of the buffer fluid. The first and second terms of (7) indicate the thermal-energy transfer due to convection and thermal diffusion, respectively. The third and fourth terms represent thermal energy generation in the system due to viscous dissipation and Joule heating, respectively. For incompressible flow in a two-dimensional straight channel the viscous dissipation term can be expressed as

$$\Phi = \mu\left(\frac{\partial u}{\partial y} + \frac{\partial v}{\partial x}\right)^2 + 2\mu\left\{\left(\frac{\partial u}{\partial x}\right)^2 + \left(\frac{\partial v}{\partial y}\right)^2\right\}. \tag{8}$$

Since we have modelled the electrokinetic component of the flow velocity with a Helmholtz-Smoluchowski slip velocity, the viscous-dissipation term is active mainly due to the pressure-driven component of the velocity. Therefore, for hydraulically fully developed mixed electro-osmotic and pressure-driven flow in a two-dimensional straight channel, the ratio of Joule heating to viscous dissipation can be expressed as

$$R_{ev} = \frac{\int_{-D}^{+D} \sigma E_x^2 \, \mathrm{d}y}{\int_{-D}^{+D} \mu (\frac{y}{\mu} \frac{\mathrm{d}P}{\mathrm{d}x})^2 \, \mathrm{d}y} \cong \frac{3}{4} \mu\sigma \left(\frac{D}{\Omega \varepsilon \zeta} \right)^2, \tag{9}$$

where Ω is the normalized pressure gradient ($\Omega = -\frac{1}{2} \frac{\mathrm{d}P^*}{\mathrm{d}\xi}$) and P^* is the non-dimensional pressure ($P^* = \frac{PD}{\mu u_{HS}}$). From Equation (9), it is clear that the ratio of generation terms, R_{ev}, is independent of the externally applied electric field, but it depends on characteristic dimensions, pressure gradient, zeta potential, and conductivity. For the flow and electrokinetic parameter ranges considered for this study, as shown in Table 2, the above ratio varies between 10 and 10000. Hence we neglect the viscous-dissipation term in this analysis. Therefore, for hydraulically fully developed mixed flow, the two-dimensional temperature equation can be written as

$$\rho_f c_p u \frac{\partial T}{\partial x} = \frac{\partial}{\partial x} \left(k \frac{\partial T}{\partial x} \right) + \frac{\partial}{\partial y} \left(k \frac{\partial T}{\partial y} \right) + \sigma E_x^2 \quad \text{in } 0 \le x < \infty, \ 0 \le y \le D, \tag{10a}$$

where E_x is the electric field along the channel. For the constant wall-heat-flux case, our microchannel system is subjected to the following boundary conditions

$$T = T_e \qquad \text{at } x = 0, \quad 0 \le y \le D, \tag{10b}$$

$$T < \infty \qquad \text{at } x \to \infty, \ 0 \le y \le D, \tag{10c}$$

$$\frac{\partial T}{\partial y} = 0 \qquad \text{at } y = 0, \quad 0 \le x < \infty, \tag{10d}$$

$$\frac{\partial T}{\partial y} = \frac{q_s''}{k} \quad \text{at } y = D, \quad 0 \le x < \infty, \tag{10e}$$

where T_e is the inlet temperature and q_s'' is the surface heat flux. When thermal energy enters into the channel, q_s'' is positive and vice versa. If we consider a case where the fluid comes into the microchannel from a reservoir, then the inlet temperature, T_e remains constant.

2.5. Normalized energy equation

We normalize Equation (10a) and present the non-dimensional temperature equation as

$$\mathrm{Pe}_T U \frac{\partial \theta}{\partial \xi} = \frac{\partial^2 \theta}{\partial \xi^2} + \frac{\partial^2 \theta}{\partial \eta^2} + G \quad \text{in } 0 \le \xi < \infty, \ 0 \le \eta \le 1 \tag{11a}$$

and the corresponding non-dimensional boundary conditions are

$$\theta = 0 \qquad \text{at } \xi = 0, \quad 0 \le \eta \le 1, \tag{11b}$$

$$\theta < \infty \qquad \text{at } \xi \to \infty, \ 0 \le \eta \le 1, \tag{11c}$$

$$\frac{\partial \theta}{\partial \eta} = 0 \quad \text{at } \eta = 0, \quad 0 \le \xi < \infty, \tag{11d}$$

$$\frac{\partial \theta}{\partial \eta} = 1 \quad \text{at } \eta = 1, \quad 0 \le \xi < \infty, \tag{11e}$$

where θ is the non-dimensional temperature, which is given by $\theta = (T - T_e)k/(Dq_s'')$. The normalized generation term, G, is presented as $G = \sigma(\vec{E} \cdot \vec{E})D/q_s''$, and it represents a ratio of

heat generated by Joule heating to surface heat rate. Hence, G is positive for heat addition into the channel and vice versa. The streamwise and cross-stream coordinates (x, y) are normalized with respect to the half channel height, D, as ($\xi = x/D$, $\eta = y/D$), and the microflow velocity is normalized with respect to the Helmholtz-Smoluchowski velocity, u_{HS}, as

$$U = \frac{u}{u_{\mathrm{HS}}} = U_{\mathrm{HS}} + U_{\mathrm{Pois}} = 1 + \Omega\left(1 - \eta^2\right) \tag{12}$$

and the corresponding mean velocity is

$$U_m = \frac{1}{A_{\mathrm{c}}}\int_{A_{\mathrm{c}}} U\,\mathrm{d}A = \int_0^1 U\,\mathrm{d}\eta = 1 + \frac{2}{3}\Omega, \tag{13}$$

where A_{c} is the cross-sectional area of the channel ($A_{\mathrm{c}} = 2WD$). The positive values of the normalized pressure gradient ($\Omega > 0$) show a favorable pressure gradient in the system (Figure 2(b)) and negative values of Ω indicate an adverse pressure gradient in the channel (Figure 2(c)). Note that in the no-pressure-gradient case, $\Omega = 0$, the resultant velocity becomes a Helmholtz–Smoluchowski electro-osmotic velocity. The thermal Peclet number, $\mathrm{Pe_T}$, is defined as

$$\mathrm{Pe_T} = \mathrm{RePr} = \left(\frac{\rho_f u_{\mathrm{HS}} D}{\mu}\right)\left(\frac{\mu c_{\mathrm{p}}}{k}\right), \tag{14}$$

where $\mathrm{Re} = \frac{\rho_f u_{\mathrm{HS}} D}{\mu}$ is the flow Reynolds number based on the Helmholtz-Smoluchowski velocity and $\mathrm{Pr} = \frac{\mu c_p}{k}$ is the fluid Prandtl number. Here, D is used as the characteristic length as opposed to the hydraulic diameter, D_{H} ($D_{\mathrm{H}} = 4D$). Hence, Reynolds, Nusselt, and Peclet numbers in this study will be one fourth of their conventional values, where those numbers are calculated based on hydraulic diameter.

3. Analysis of the normalized energy equation

3.1. Fully developed temperature distribution

In the fully developed region, the constant-heat-flux condition at the wall yields

$$\left.\frac{\partial\theta}{\partial\xi}\right|_{\mathrm{fd}} = \left.\frac{\mathrm{d}\theta_{\mathrm{s}}}{\mathrm{d}\xi}\right|_{\mathrm{fd}} = \left.\frac{\mathrm{d}\theta_{\mathrm{m}}}{\mathrm{d}\xi}\right|_{\mathrm{fd}} = \mathrm{const}, \tag{15}$$

where the subscript fd indicates the fully developed region, θ_{s} is the normalized surface temperature, and θ_{m} is the normalized bulk mean temperature. In the fully developed region, the governing equation for the constant-wall-heat-flux case becomes

$$\mathrm{Pe_T} U \left.\frac{\mathrm{d}\theta_{\mathrm{m}}}{\mathrm{d}\xi}\right|_{\mathrm{fd}} = \left.\frac{\partial^2\theta}{\partial\eta^2}\right|_{fd} + G \quad \text{in } 0 \le \xi < \infty,\ \ 0 \le \eta \le 1 \tag{16a}$$

and corresponding boundary conditions are

$$\left.\frac{\partial\theta}{\partial\eta}\right|_{\mathrm{fd}} = 0 \quad \text{at } \eta = 0,\ \ 0 \le \xi < \infty, \tag{16b}$$

$$\left.\frac{\partial\theta}{\partial\eta}\right|_{\mathrm{fd}} = 1 \quad \text{at } \eta = 1,\ \ 0 \le \xi < \infty. \tag{16c}$$

Integrating (16a) twice with respect to η, we obtain

$$\theta_{\mathrm{fd}} = \mathrm{Pe_T} \frac{\mathrm{d}\theta_{\mathrm{m}}}{\mathrm{d}\xi}\bigg|_{\mathrm{fd}} \left\{ \frac{1}{2}(1+\Omega)\eta^2 - \frac{\Omega}{12}\eta^4 \right\} - \frac{G}{2}\eta^2 + C_1\eta + C_2, \tag{17}$$

where C_1 and C_2 are constants or functions of ξ. Applying boundary conditions, (16b) and (16c), yields $C_1 = 0$ and $(\mathrm{d}\theta_{\mathrm{m}}/\mathrm{d}\xi)|_{\mathrm{fd}} = (1+G)/(\mathrm{Pe_T} U_{\mathrm{m}})$, respectively. Therefore, the normalized mean temperature in the fully developed region becomes

$$\theta_{\mathrm{m}}|_{\mathrm{fd}} = \frac{1+G}{\mathrm{Pe_T} U_{\mathrm{m}}}\xi + C_3, \tag{18}$$

where C_3 is an arbitrary constant, and for simplicity we assume $C_3 = 0$. Now substituting (18) in (17) gives

$$\theta_{\mathrm{fd}} = \frac{1+G}{U_{\mathrm{m}}} \left\{ \frac{1}{2}(1+\Omega)\eta^2 - \frac{\Omega}{12}\eta^4 \right\} - \frac{G}{2}\eta^2 + C_2. \tag{19}$$

Again from (19), we can obtain an expression for the mean temperature in the fully developed region as

$$\begin{aligned} \theta_{\mathrm{m}}|_{\mathrm{fd}} &= \frac{1}{U_{\mathrm{m}} A_{\mathrm{c}}} \int_{A_{\mathrm{c}}} U\theta_{\mathrm{fd}}\, \mathrm{d}A = \frac{1}{U_{\mathrm{m}}} \int_0^1 U\theta_{\mathrm{fd}}\, \mathrm{d}\eta \\ &= \frac{1+G}{U_{\mathrm{m}}^2}\left(\frac{70+91\Omega+26\Omega^2}{420} \right) - \frac{G}{6U_{\mathrm{m}}}\left(1 + \frac{2}{5}\Omega \right) + C_2. \end{aligned} \tag{20}$$

By equating (18) and (20), C_2 can be obtained as

$$C_2 = \frac{1+G}{U_{\mathrm{m}}^2}\left(\frac{\xi}{\mathrm{Pe_T}} - \frac{70+91\Omega+26\Omega^2}{420} \right) + \frac{G}{2}\left(\frac{5+2\Omega}{15U_{\mathrm{m}}} \right). \tag{21}$$

Therefore, the normalized temperature in fully developed region is

$$\theta_{\mathrm{fd}} = \frac{1+G}{U_{\mathrm{m}}^2} \left\{ \frac{1}{2}(1+\Omega)\eta^2 - \frac{\Omega}{12}\eta^4 + \frac{\xi}{\mathrm{Pe_T}} - \frac{70+91\Omega+26\Omega^2}{420} \right\} + \frac{G}{2}\left(\eta^2 - \frac{5+2\Omega}{15U_{\mathrm{m}}} \right). \tag{22}$$

Since we set $C_3 = 0$ in (18), the fully developed temperature expression presented by (22) is not a unique solution, but rather a particular solution. This particular solution will be used in the next section to obtain a unique solution for the whole domain.

3.2. Heat transfer characteristics in the mixed flow

Since Equation (11a) is not separable, due to the presence of η in the velocity distribution, the standard separation of variables technique cannot be applied. Hence, the extended Graetz problem is considered to obtain the temperature distribution in both developing and fully developed regions. The total temperature solution can be decomposed as

$$\theta = \theta_{\mathrm{p}} + \theta_g, \tag{23}$$

where θ_{p} is the particular solution, and it has been chosen such that the homogeneous solution, θ_g, satisfies a homogeneous equation. Note that a particular solution, θ_{p}, can be any function as long as a general solution exists. For this particular study, let us take the fully developed temperature obtained in the previous section as the particular solution ($\theta_{\mathrm{p}} = \theta_{\mathrm{fd}}$). Thus, the associated governing equation for θ_g becomes

$$\mathrm{Pe_T} U \frac{\partial\theta_g}{\partial\xi} = \frac{\partial^2\theta_g}{\partial\xi^2} + \frac{\partial^2\theta_g}{\partial\eta^2} \quad \text{in } 0 \le \xi < \infty,\ \ 0 \le \eta \le 1 \tag{24a}$$

and the corresponding boundary conditions are

$$\theta_g = -\theta_{\mathrm{fd}}|_{\xi=0} \quad \text{at } \xi = 0, \quad 0 \le \eta \le 1, \tag{24b}$$

$$\theta_g < \infty \quad \text{at } \xi \to \infty, \quad 0 \le \eta \le 1, \tag{24c}$$

$$\frac{\partial \theta_g}{\partial \eta} = 0 \quad \text{at } \eta = 0, \quad 0 \le \xi < \infty, \tag{24d}$$

$$\frac{\partial \theta_g}{\partial \eta} = 0 \quad \text{at } \eta = 1, \quad 0 \le \xi < \infty. \tag{24e}$$

Suppose the solution to the boundary-value problem (24) is of the form [22]:

$$\theta_g = \sum_{n=1}^{\infty} A_n f_n(\eta) \exp\left[-\frac{\lambda_n^2}{\mathrm{Pe}_T}\xi\right] \quad \text{in } 0 \le \xi < \infty, \quad 0 \le \eta \le 1, \tag{25}$$

where A_n are the coefficients, f_n are the eigenfunctions, and λ_n are the eigenvalues. Substituting (25) in (24), we obtain the following nonlinear eigenvalue problem

$$\frac{\mathrm{d}^2 f_n}{\mathrm{d}\eta^2} + \lambda_n^2 \left\{ \left(\frac{\lambda_n}{\mathrm{Pe}_T} \right)^2 + U \right\} f_n = 0 \quad \text{in } 0 < \eta < 1, \tag{26a}$$

$$\frac{\mathrm{d} f_n}{\mathrm{d}\eta} = 0 \quad \text{at } \eta = 0, \tag{26b}$$

$$\frac{\mathrm{d} f_n}{\mathrm{d}\eta} = 0 \quad \text{at } \eta = 1. \tag{26c}$$

The solution of (26a) subject to the symmetric boundary condition, (26b), can be expressed as

$$f_n = \exp\left[-\frac{1}{2}\lambda_n \sqrt{\Omega}\eta^2\right] \; {}_1F_1(a; b; z) \tag{27}$$

where ${}_1F_1(a; b; z) = \sum_{n=0}^{\infty} (a)_n/(b)_n z^n/n!$ is the Kummer confluent hypergeometric function, and

$$a = \frac{-\lambda_n^3 - \mathrm{Pe}_{\mathrm{T}}^2\{\lambda_n(1+\Omega) - \sqrt{\Omega}\}}{4\sqrt{\Omega}\mathrm{Pe}_T^2}, \quad b = \frac{1}{2}, \quad z = \lambda_n \sqrt{\Omega}\eta^2.$$

Here $(a)_n$ and $(b)_n$ are known as the Pochhammer symbols. The eigenfunctions $\{f_n\}$ presented by (27) has a sequence of eigenvalues $\{\lambda_n\}$, and $\{f_n\}_{n=1}^{\infty}$ form a base for the function space $L^2(0, 1)$. Our next goal is to find the eigenvalues $\{\lambda_n\}$ from (27) by utilizing the wall boundary condition given in (26c). For this nonlinear eigenvalue problem, the Secant method is utilized to find out the corresponding eigenvalues. Note that the eigenfunctions $\{f_n\}$ are not mutually orthogonal (when compared to the standard Sturm-Liouville problem) since the eigenvalues $\{\lambda_n\}$ occur nonlinearly in (26a). We use the Gram-Schmidt orthogonal procedure [30, Chapter 9] in order to determine the coefficients, $\{A_n\}$, from a set of linearly independent eigenfunctions $\{f_n\}_{n=1}^{\infty}$ as follows:

$$A_n = B_n - \sum_{j=n+1}^{N} \alpha_{jn} B_j \tag{28}$$

with

$$B_n = -\left(\int_0^1 g_n \theta_{fd}|_{\xi=0} \, \mathrm{d}\eta\right) \Big/ \left(\int_0^1 g_n^2 \, \mathrm{d}\eta\right), \quad g_n = f_n - \sum_{j=1;n\ge 2}^{n-1} \alpha_{nj} f_j, \quad \alpha_{ij} = \frac{\langle f_i, f_j \rangle}{\|f_j\|^2},$$

where N is a sufficiently large number to represent infinity, $\|\cdot\|$ represents the norm of $L^2(0, 1)$ space, and g_n is a series of orthogonal functions.

The complete solution to the original governing equation (11a) can be obtained as follows by combining (22), (23), and (25)

$$\theta = \theta_{\mathrm{fd}} + \theta_g = \frac{1+G}{U_{\mathrm{m}}^2}\left\{\frac{1}{2}(1+\Omega)\eta^2 - \frac{\Omega}{12}\eta^4 + \frac{\xi}{\mathrm{Pe_T}} - \frac{70+91\Omega+26\Omega^2}{420}\right\} + \frac{G}{2}\left(\eta^2 - \frac{5+2\Omega}{15U_{\mathrm{m}}}\right) + \sum_{n=1}^{\infty} A_n f_n \exp\left[-\frac{\lambda_n^2}{\mathrm{Pe_T}}\xi\right] \tag{29}$$

and the corresponding normalized bulk mean temperature becomes

$$\theta_{\mathrm{m}} = \theta_{\mathrm{m}}|_{\mathrm{fd}} + \theta_{\mathrm{m}}|_g = \frac{1+G}{\mathrm{Pe_T}U_{\mathrm{m}}}\xi + \frac{1}{U_{\mathrm{m}}}\sum_{n=1}^{\infty} A_n \exp\left[-\frac{\lambda_n^2}{\mathrm{Pe_T}}\xi\right]\int_0^1 U f_n \mathrm{d}\eta. \tag{30}$$

The imposed heat flux at the wall can be found from Newton's law of cooling as

$$q_{\mathrm{s}}'' = h(T_{\mathrm{s}} - T_{\mathrm{m}}), \tag{31}$$

where h is the local heat-transfer coefficient and T_{s} is the wall temperature. The normalized surface temperature can be expressed as

$$\theta_{\mathrm{s}} = \theta_{\mathrm{s}}|_{\mathrm{fd}} + \theta_{\mathrm{s}}|_g = \frac{1+G}{U_{\mathrm{m}}}\left(\frac{1}{2} + \frac{5}{12}\Omega + \frac{\xi}{\mathrm{Pe_T}} - \frac{70+91\Omega+26\Omega^2}{420}\right) - \frac{G}{2}\left(1 - \frac{5+2\Omega}{15U_{\mathrm{m}}}\right) + \sum_{n=1}^{\infty} A_n \exp[-\frac{\lambda_n^2}{\mathrm{Pe_T}}\xi] f_n|_{\eta=1}. \tag{32}$$

The Nusselt number can be derived from (30) to (32) as

$$\mathrm{Nu}_\xi = \frac{Dh}{k} = \frac{1}{\theta_{\mathrm{s}} - \theta_{\mathrm{m}}} = 35(3+2\Omega)^2 \times \left[105+14(12+G)\Omega+4(17+3G)\Omega^2+35(3+2\Omega)\sum_{n=1}^{\infty} A_n \exp[-\tfrac{\lambda_n^2}{\mathrm{Pe_T}}\xi]\{(3+2\Omega) f_n|_{\eta=1} - 3\int_0^1 U f_n \mathrm{d}\eta\}\right]^{-1}. \tag{33}$$

4. Discussion of results

The heat-transfer characteristics of mixed electro-osmotic and pressure-driven flows are quantified by (29–33). The eigenfunctions used in this study are not orthogonal and they contain hypergeometric functions. Hence, the Gram-Schmidt orthogonalization procedure is considered in order to find the coefficients, A_n. The first 20 values of the eigenvalues, λ_n, and corresponding coefficients, A_n, for $\Omega = 0$, 0·5, and $-0{\cdot}5$ are listed in Table 3 for $\mathrm{Pe_T} = 5$. Even though our solution can be used for any values of the Peclet number, we have presented only low-Peclet-number cases primarily due to their relevance to the microdevices. All temperature distributions are presented in this study for de-ionized water at $\mathrm{Pe_T} = 5$, $\mathrm{Pr} = 7$, and $D > 1000\lambda$. Therefore, the hydrodynamic entry length is negligible, and the fully developed velocity is justified right from the beginning of the channel.

In our previous study [27], we have reported results on the thermal behavior of pure electroosmotic flow in both (thermally) developing and fully developed regions. Here we present the heat-transfer characteristics in mixed flow cases. Two different mixed flow cases are considered for this study: favorable pressure-driven and adverse pressure-driven. For favorable

Table 3. First 20 terms of coefficients (A_n) and corresponding eigenvalues (λ_n) for $\mathrm{Pe_T} = 5$.

	$\Omega = -0{\cdot}5$		$\Omega = 0{\cdot}0$		$\Omega = +0{\cdot}5$	
n	λ_n	A_n	λ_n	A_n	λ_n	A_n
1	3·064	$+1{\cdot}9\times10^{-1}-3{\cdot}3\times10^{-2}G$	2·752	$+2{\cdot}0\times10^{-1}$	2·521	$+2{\cdot}1\times10^{-1}+1{\cdot}5\times10^{-2}G$
2	4·915	$-4{\cdot}6\times10^{-2}+9{\cdot}7\times10^{-4}G$	4·616	$-5{\cdot}1\times10^{-2}$	4·355	$-5{\cdot}4\times10^{-2}-1{\cdot}3\times10^{-3}G$
3	6·287	$+2{\cdot}1\times10^{-2}-1{\cdot}9\times10^{-4}G$	6·021	$+2{\cdot}3\times10^{-2}$	5·776	$+2{\cdot}4\times10^{-2}+2{\cdot}5\times10^{-4}G$
4	7·420	$-1{\cdot}1\times10^{-2}+6{\cdot}5\times10^{-5}G$	7·181	$-1{\cdot}3\times10^{-2}$	6·955	$-1{\cdot}3\times10^{-2}-7{\cdot}4\times10^{-5}G$
5	8·406	$+7{\cdot}5\times10^{-3}-2{\cdot}8\times10^{-5}G$	8·187	$+8{\cdot}1\times10^{-3}$	7·978	$+8{\cdot}5\times10^{-3}+2{\cdot}9\times10^{-5}G$
6	9·289	$-5{\cdot}3\times10^{-3}+1{\cdot}4\times10^{-5}G$	9·087	$-5{\cdot}6\times10^{-3}$	8·892	$-5{\cdot}9\times10^{-3}-1{\cdot}3\times10^{-5}G$
7	10·096	$+3{\cdot}9\times10^{-3}-7{\cdot}9\times10^{-6}G$	9·908	$+4{\cdot}1\times10^{-3}$	9·724	$+4{\cdot}3\times10^{-3}+7{\cdot}0\times10^{-6}G$
8	10·845	$-3{\cdot}0\times10^{-3}+4{\cdot}7\times10^{-6}G$	10·667	$-3{\cdot}1\times10^{-3}$	10·493	$-3{\cdot}3\times10^{-3}-3{\cdot}9\times10^{-6}G$
9	11·545	$+2{\cdot}4\times10^{-3}-3{\cdot}0\times10^{-6}G$	11·376	$+2{\cdot}5\times10^{-3}$	11·212	$+2{\cdot}6\times10^{-3}+2{\cdot}4\times10^{-6}G$
10	12·206	$-2{\cdot}0\times10^{-3}+2{\cdot}0\times10^{-6}G$	12·045	$-2{\cdot}0\times10^{-3}$	11·887	$-2{\cdot}1\times10^{-3}-1{\cdot}5\times10^{-6}G$
11	12·832	$+1{\cdot}6\times10^{-3}-1{\cdot}4\times10^{-6}G$	12·678	$+1{\cdot}7\times10^{-3}$	12·527	$+1{\cdot}7\times10^{-3}+9{\cdot}9\times10^{-7}G$
12	13·430	$-1{\cdot}4\times10^{-3}+9{\cdot}9\times10^{-7}G$	13·282	$-1{\cdot}4\times10^{-3}$	13·137	$-1{\cdot}4\times10^{-3}-6{\cdot}8\times10^{-7}G$
13	14·002	$+1{\cdot}2\times10^{-3}-7{\cdot}2\times10^{-7}G$	13·860	$+1{\cdot}2\times10^{-3}$	13·720	$+1{\cdot}2\times10^{-3}+4{\cdot}8\times10^{-7}G$
14	14·551	$-1{\cdot}0\times10^{-3}+5{\cdot}4\times10^{-7}G$	14·414	$-1{\cdot}0\times10^{-3}$	14·279	$-1{\cdot}1\times10^{-3}-3{\cdot}4\times10^{-7}G$
15	15·081	$+8{\cdot}8\times10^{-4}-4{\cdot}1\times10^{-7}G$	14·948	$+9{\cdot}0\times10^{-4}$	14·817	$+9{\cdot}2\times10^{-4}+2{\cdot}5\times10^{-7}G$
16	15·593	$-7{\cdot}7\times10^{-4}+3{\cdot}2\times10^{-7}G$	15·464	$-7{\cdot}9\times10^{-4}$	15·337	$-8{\cdot}1\times10^{-4}-1{\cdot}9\times10^{-7}G$
17	16·088	$+6{\cdot}9\times10^{-4}-2{\cdot}5\times10^{-7}G$	15·963	$+7{\cdot}0\times10^{-4}$	15·840	$+7{\cdot}1\times10^{-4}+1{\cdot}4\times10^{-7}G$
18	16·569	$-6{\cdot}1\times10^{-4}+2{\cdot}0\times10^{-7}G$	16·448	$-6{\cdot}3\times10^{-4}$	16·327	$-6{\cdot}4\times10^{-4}-1{\cdot}1\times10^{-7}G$
19	17·036	$+5{\cdot}5\times10^{-4}-1{\cdot}6\times10^{-7}G$	16·918	$+5{\cdot}6\times10^{-4}$	16·800	$+5{\cdot}7\times10^{-4}+8{\cdot}5\times10^{-8}G$
20	17·491	$-5{\cdot}0\times10^{-4}+1{\cdot}3\times10^{-7}G$	17·376	$-5{\cdot}1\times10^{-4}$	17·261	$-5{\cdot}2\times10^{-4}-6{\cdot}7\times10^{-8}G$

pressure-driven mixed flows ($\Omega > 0$) the pressure gradient, $\dfrac{\mathrm{d}P}{\mathrm{d}x}$, is negative, while the pressure gradient is positive for adverse pressure-driven mixed flows ($\Omega < 0$). Based on the thermal conditions, three different scenarios ($G = 1, -1$ and -2) are explored. For $G = 1$ and $G = -1$, the amount of heat addition to the channel and heat rejection from the channel is same as heat generation, respectively. On the other hand, $G = -2$ presents the case where heat generation is twice the amount of heat rejected. It is important to note that our analytical results are valid for any finite value of normalized source term including negligible generation term for which $G \to 0$.

4.1. Mixed flow with favorable pressure gradient

Figures 3 and 4 show the temperature distribution for favorable pressure-gradient flow at $\Omega = 0{\cdot}5$. This is a representative case where external pressure head is applied along the electro-osmotic flow direction. In this case, the contribution of pressure-driven flow is one-third of the pure electro-osmotic flow. Therefore, the discharge of mixed flow is 1·333 times higher than that of pure electro-osmotic case. Due to the geometric, hydrodynamic, and thermal symmetry, the results are presented for only the upper half of the channel.

The normalized wall-temperature distributions for favorable pressure-gradient mixed flow ($\Omega = 0{\cdot}5$) are illustrated in Figure 3 for different normalized source terms. The dimensional surface temperature ($T_\mathrm{s} = T_\mathrm{e} + \theta_\mathrm{s} q''_\mathrm{s} D/k$) changes along the downstream direction of the microchannel. For positive value of G, the surface temperature will increase due to both heat generation in the entire volume and heat addition through the top and bottom walls. However,

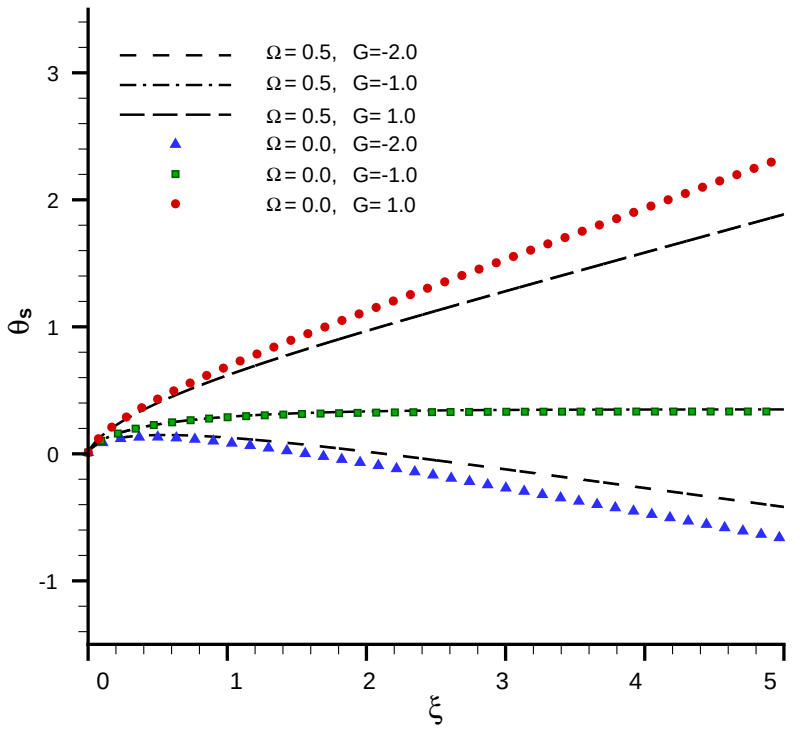

Figure 3. Normalized wall temperature, θ_s, distribution along the channel in pure ($\Omega = 0$) and favorable-pressure-gradient mixed ($\Omega = 0{\cdot}5$) flows for $Pe_T = 5{\cdot}0$.

for negative values of G, the surface temperature may increase or decrease depending on the relative magnitude of energy generation to heat rejection. For example, for $G = -2$ the dimensional surface temperature increases in the downstream direction since the amount of heat rejection is half of the heat generation due to Joule heating. On the other hand, at $G = -1$, the amount of Joule heat is equal to the surface heat rejection. Therefore, for the $G = -1$ case, the surface temperature does not change after the entry region. In all cases, the slope of the surface temperature becomes constant once the flow becomes thermally fully developed and for that reason the wall temperature has been plotted up to $\xi = 5$. Although the non-dimensional wall temperature can change a few orders of magnitude in the downstream direction (for $G \neq -1$), the dimensional temperature change ($T_s - T_e$) is less than 5K due to the conversion factor $q_s'' D/k = 5 \times 10^{-4} K$, even for an external electric field, $|\vec{E}| = 10$ V/mm, and electrical conductivity, 300 μS/m in a 20 μm deep channel. Therefore, temperature independence on fluid properties can be justified at any section of the channel.

The normalized surface temperature distributions for pure electro-osmotic flow ($\Omega = 0$) are also shown in Figure 3. At any particular position and for a particular value of the normalized source term, the dimensional wall temperature (T_s) in a favorable-pressure-gradient mixed flow case is smaller than that of pure electro-osmotic flow. This is primarily due to a higher volume flow rate associated with the mixed flow case considered here.

For the above-mentioned mixed flow case, the normalized temperature difference, $\Delta\theta = \theta_s - \theta$, distributions across the channel are plotted in Figure 4 at different axial locations. The convergence of the infinite series is very slow at $\xi = 0$, and hence we have plotted our results from $\xi = 0{\cdot}1$. Unlike pure electro-osmotic flow [27], the $\Delta\theta$ distribution is dependent on the generation term, but the general trend of the normalized temperature difference distribution

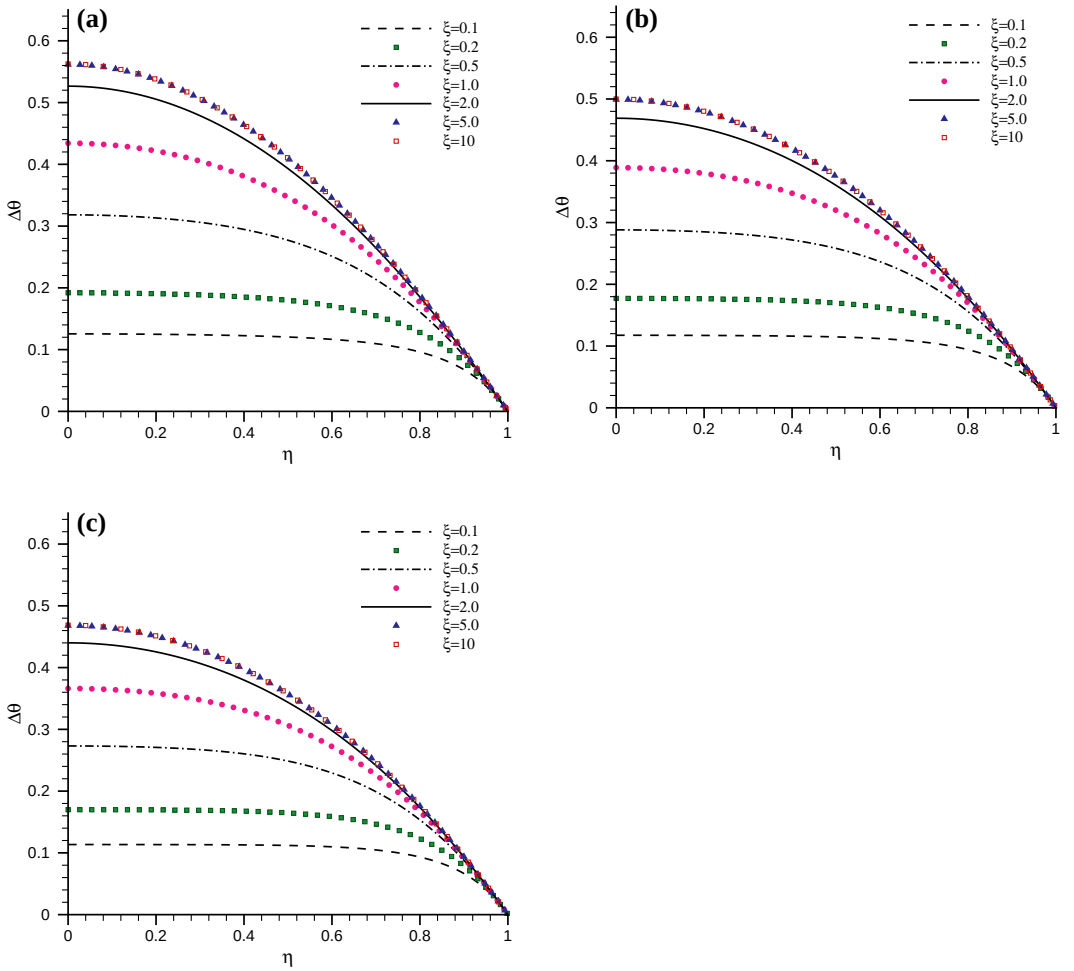

Figure 4. Non-dimensional temperature difference, $\Delta\theta = \theta_s - \theta$, across the channel in favorable-pressure-driven mixed flow ($\Omega = 0{\cdot}5$) at different downstream locations, ξ, for $Pe_T = 5{\cdot}0$ and for (a) $G = 1$, (b) $G = -1$, and (c) $G = -2$.

remains the same for both positive and negative values of G. It is noteworthy to mention that the dimensional temperature difference, $\Delta T = T_s - T$, profile should not be identical for both positive and negative values of the normalized source term. For positive values of the normalized source term ($G > 0$) at any particular section, the surface temperature is higher than the fluid temperature to maintain a positive heat flux. However, for negative values of the normalized source term ($G < 0$), the surface temperature is less than the fluid temperature to remove heat from the system. As the flow proceeds along the channel, the non-dimensional temperature difference increases, especially at the centerline ($y = 0$), until it reaches a constant value in the fully developed region as shown in Figure 4. However, the dimensional temperature, $T(x, y)$, distribution changes along the channel since the wall temperature, $T_s(x)$, varies in the downstream direction.

The fully developed $\Delta\theta$ at the centerline increases with the normalized source term. This is mainly due to the net difference in the heat generation and heat transfer at the top and bottom walls. Analytical results (not shown in the figure) also indicate that the value of the normalized temperature difference at the centerline ($\Delta\theta_c = \theta_s - \theta_c$) will be even larger for higher values of Ω. This indicates weaker heat-transfer characteristics for higher values of the applied

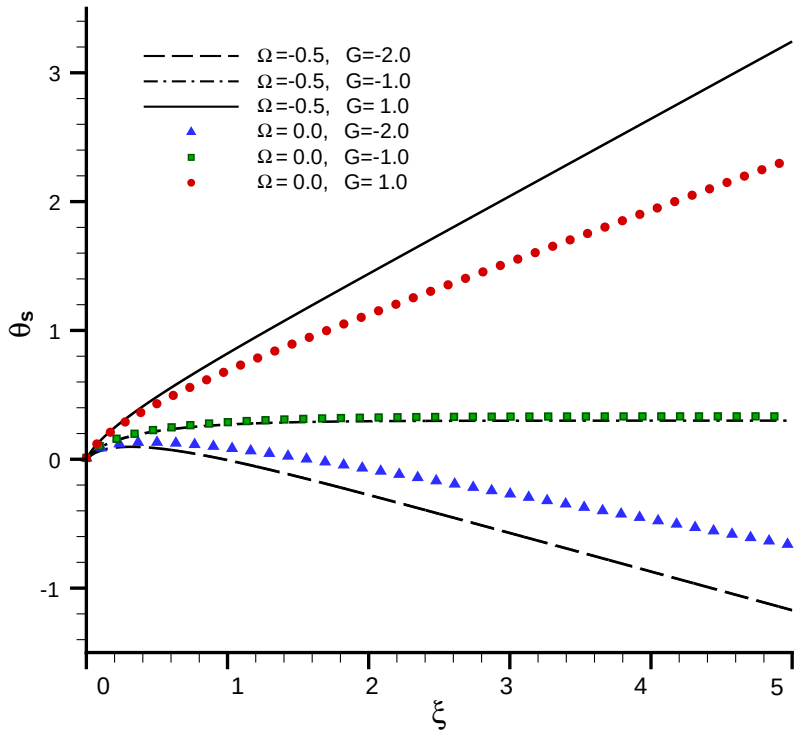

Figure 5. Normalized wall temperature, θ_s, distribution along the channel in pure ($\Omega = 0$) and adverse-pressure-gradient mixed ($\Omega = -0{\cdot}5$) flows for $Pe_T = 5{\cdot}0$.

pressure gradient in the flow direction. The weaker heat-transfer performance can be attributed to the parabolic velocity profile obtained from the applied pressure gradient. As the pressure gradient increases, the parabolic contribution becomes dominant, which affects the temperature profile, especially at the center of the channel.

4.2. Mixed flow with adverse pressure gradient

Figure 5 shows the normalized surface-temperature distribution along the channel for $\Omega = -0{\cdot}5$. A negative value of Ω corresponds to an adverse pressure gradient flow where there is a net gain in the pressure head. This net pressure gain could be used to drive the micro-flow in the electro-osmotically suppressed region [28]. Moreover, in the absence of any external forcing mechanism, the adverse-pressure-gradient case is used to compensate any pressure drop in the corners and turns. Even though adverse-pressure-gradient flow provides net pressure head in the microfluidic systems for additional pumping, the resulting net discharge is less than in the corresponding pure electro-osmotic case. For example, at $\Omega = -0{\cdot}5$, the discharge is only 66% of the pure electro-osmotic flow. Like in the favorable-pressure-gradient case, three different normalized source term values ($G = 1$, -1 and -2) are presented in Figure 5. The overall trend in the wall temperature remains the same as in the favorable-pressure-gradient case. However, in this case the dimensional surface temperature at any particular position is higher than that of pure electro-osmotic flow. This is due to the lower flow rate associated with the adverse-pressure-gradient mixed flow.

The normalized temperature difference, $\Delta\theta = \theta_s - \theta$, for the above-mentioned mixed flow case ($\Omega = -0{\cdot}5$) is illustrated in Figure 6. Like in the favorable-pressure-gradient mixed flow, the non-dimensional temperature difference at any lateral location (y) keeps increasing until

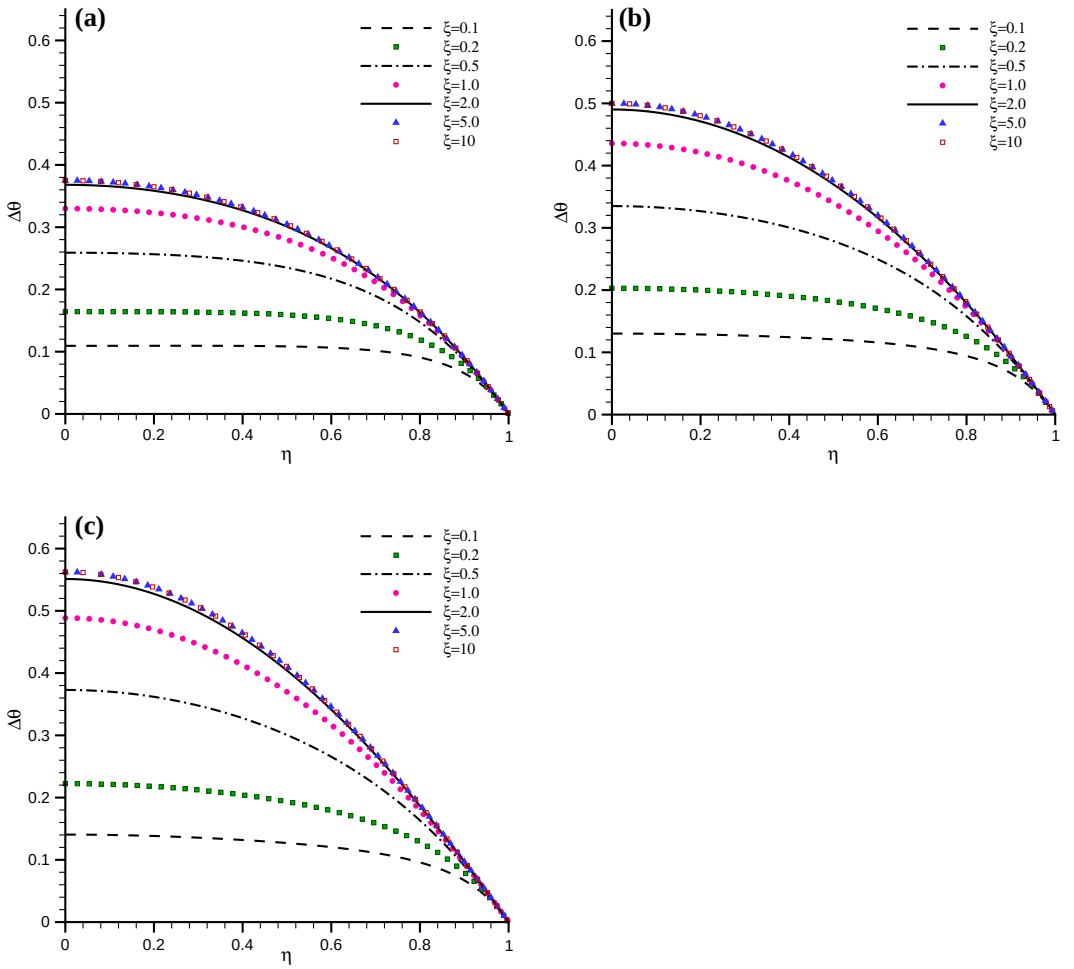

Figure 6. Non-dimensional temperature difference, $\Delta\theta = \theta_s - \theta$, across the channel in adverse-pressure-driven mixed flow ($\Omega = -0{\cdot}5$) at different downstream locations, ξ, for $Pe_T = 5{\cdot}0$ and for (a) $G = 1$, (b) $G = -1$, and (c) $G = -2$.

the flow becomes thermally fully developed. Moreover, the normalized temperature difference at any particular location is a function of normalized source term. Here a positive value of the normalized source term ($G = 1$) provides less non-dimensional temperature difference in the fluid than that of a favorable-pressure-driven flow ($\Omega = 0{\cdot}5$) case. This implies that, at any particular location, the difference in surface and fluid temperature ($T_s - T$) is less than that of a favorable-pressure-gradient flow. Hence, for $G = 1$, the fluid temperature at any position will be higher in an adverse-pressure-gradient mixed flow than that of pure electro-osmotic or favorable-pressure-gradient mixed flow. Similarly, for the $G = -2$ case, the dimensional fluid temperature at any location is higher for the adverse-pressure-gradient case than that of favorable-pressure-gradient case. In other words, the effects of Joule heating becomes more dominant as the flow rate becomes smaller. For this reason, the thermal entry length is much shorter when an adverse pressure gradient is imposed on pure electro-osmotic flow. Note that, in the fully developed region, the dimensional temperature difference (ΔT) is independent of Ω for $G = -1$, although the entry region is longer when a favorable-pressure-gradient is applied to electro-osmotic flow.

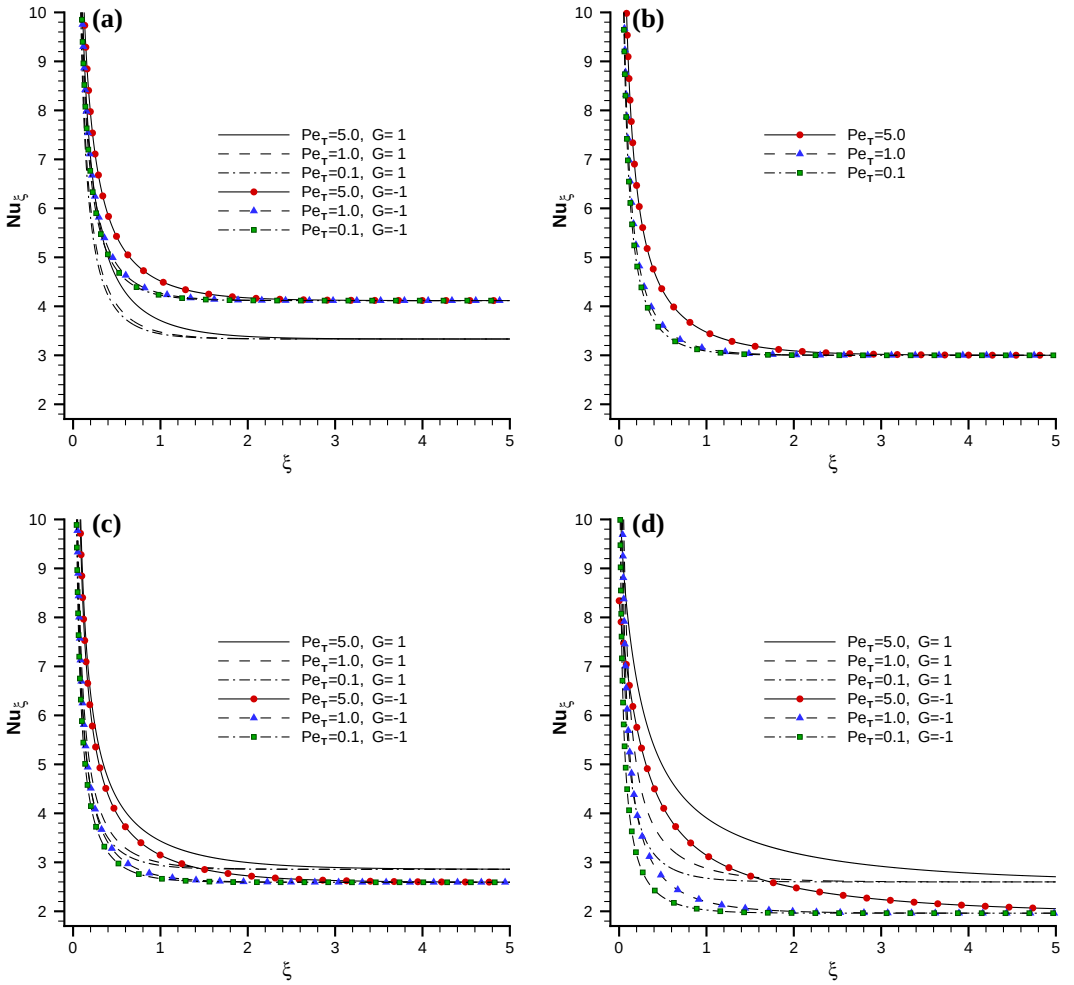

Figure 7. Local Nusselt number distribution along the channel for different normalized generation terms at various Peclet numbers for (a) $\Omega = -0{\cdot}5$, (b) $\Omega = 0{\cdot}0$, (c) $\Omega = 0{\cdot}5$, and (d) $\Omega = 5{\cdot}0$. In pure electro-osmotic flow, the Nusselt number is independent of normalized generation term.

4.3. Nusselt number

The local-Nusselt-number distributions along the channel for different mixed flow cases ($\Omega = -0{\cdot}5$, 0, 0·5, and 5·0) are presented in Figure 7 for a normalized source term $G = -1$ and 1 and for various Peclet numbers. Due to the constancy of the local Nusselt number after reaching the fully developed condition, they have been presented for up to five characteristic lengths (D). For all cases, the Nusselt number is very high at the entry and it decays abruptly as the flow proceeds. The rationale for abrupt decay of the Nusselt number is that the thermal boundary layer develops very fast along the flow direction in the microchannel. The local-Nusselt-number distribution along the channel identifies the thermal entry length, where the temperature keeps developing with ξ. In the mixed flow case, this entry length does not depend on the non-dimensional source term, G, but depends on the Peclet number, $\mathrm{Pe_T}$, and the non-dimensional pressure gradient, Ω. Figure 7 indicates that a large $\mathrm{Pe_T}$ or Ω makes the entrance length longer. In case of pure electro-osmotic flow ($\Omega = 0$), the Nusselt-number distribution is independent of G in both the fully developed and the developing region.

Table 4. Comparison of Nusselt number (based on hydraulic diameter) in the fully developed region for low Peclet number ($Pe_T = 5$) with the existing literature.

	$G = -1$		$G = 0$		$G = +1$	
	This study	Reference	This study	Reference	This study	Reference
Mixed flow ($\Omega = -0{\cdot}5$)	13·33	–	14·74	–	16·47	–
Pure electroosmotic flow	12·00	12·00 [15], [27]	12·00	12·00 [31]	12·00	12·00 [15]
Mixed flow ($\Omega = +0{\cdot}5$)	11·43	–	10·87	–	10·37	–
Mixed flow ($\Omega = +1{\cdot}0$)	11·11	–	10·26	–	9·54	–
Mixed flow ($\Omega = +5{\cdot}0$)	10·40	–	8·95	–	7·85	–
Pure Poiseulle flow	10·00	–	8·24	–	7·00	–

However, for favorable-pressure-gradient mixed flow ($\Omega > 0$), higher values of G yield less heat transfer, but for adverse-pressure-gradient mixed flow ($\Omega < 0$), a higher value of G provides higher heat transfer.

In the fully developed region, the Nusselt number becomes independent of the Peclet number and its specific values are given in Table 4 for different values of G and Ω. The fully developed Nusselt numbers are also compared with the existing values for identical geometric, electrokinetic and thermal conditions. In Table 4, our Nusselt number values are computed based on hydraulic diameter ($Nu_{D_h} = 4Nu_D$). For the pure electro-osmotic case ($\Omega = 0$), the fully developed Nusselt number reaches a value of 12·0 for any value of the non-dimensional generation term, G. On the other hand, for the mixed flow case the fully developed

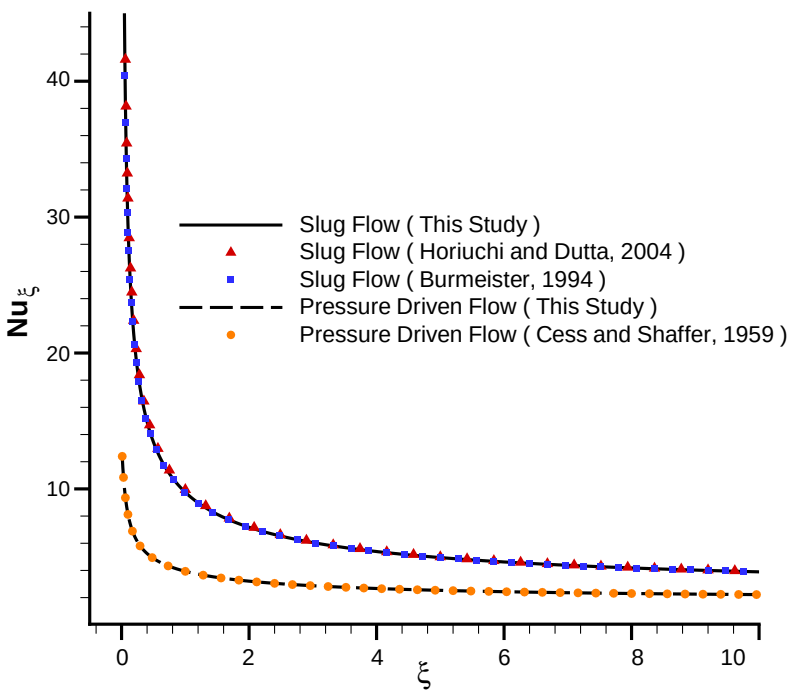

Figure 8. Local-Nusselt-number distribution along the channel for both slug flow and pressure-driven flow for $Pe_T = 100$ with no Joule heating ($G = 0$).

Nusselt number depends on the magnitude of the source term. The Nusselt number of pure electro-osmotic flow is much higher than the Poiseuille flow due to the plug-like velocity profile in the pure electro-osmotic flow. For a particular value of G, the Nusselt number of favorable-pressure-driven mixed flow is located between that of pure electro-osmotic flow and pressure-driven flow. But for adverse-pressure-driven mixed flow, the fully developed Nusselt number is even higher than that of pure electro-osmotic flow. There are two causes contributing to such high heat-transfer coefficients in adverse-pressure-gradient mixed flow. First, the velocity distribution next to the wall is plug-like. Second, the flow rate in adverse-pressure-gradient flow is less than that of pure electro-osmotic flow. Table 4 shows that in the fully developed region our results exactly match with the other existing studies for pure electro-osmotic flow.

In Figure 8 we have plotted the Nusselt-number distribution along the channel for the no-Joule-heating case at high Peclet number ($\mathrm{Pe_T} = 100$). Both slug and Poiseuille flows are considered in this case. We also compared our Nusselt-number distribution in the developing region with the existing results of Burmeister [31, Chapter 6] and Cess and Shaper [32] for slug flow and Poiseuille flows, respectively. An excellent agreement is obtained between existing data and our results in both the developing and the fully developed regions. Thus, our technique can be used to analyze macro flows where the axial conduction term can be neglected due to the very high thermal Peclet number. Figure 8 also confirms that our mathematical techniques can be used for any kind of velocity distribution with or without volumetric Joule heating. Here it is important to note that the Nusselt number of slug flow is higher than that of pressure-driven flow even in macroscale laminar flow.

5. Conclusions

We obtained analytical solutions for the heat-transfer characteristics of mixed electro-osmotic and pressure-driven flow in two-dimensional straight microchannels. The extended Greatz problem was considered to obtain the thermal behavior of low-Peclet-number microflows. Our thermal analysis under constant wall heat flux resulted in the following:

- In a mixed electro-osmotic and pressure-driven flow, the local fluid and wall temperature increase along the channel for a positive source term. On the other hand, the local fluid and wall temperature can increase or decrease for a negative source term, except for $G = -1$.
- For mixed flow of $G = -1$, both wall and fluid temperatures stop developing in the fully developed region due to the thermal-energy balance between heat generation and heat rejection.
- In mixed flow, the Nusselt number is a function of the normalized source term. But in pure electro-osmotic flow, the Nusselt number does not depend on the magnitude of the source term.
- The fully developed Nusselt number for mixed flow is independent of the thermal Peclet number if the generation term remains the same.
- For favorable-pressure-gradient mixed flow, a higher value of the non-dimensional pressure gradient makes the thermal entrance length longer, while in adverse-pressure-gradient mixed flow the entrance length will be shorter as the pressure gradient increases.
- Under a no-heat-generation case, our results verify the Nusselt number of classical slug flows and Poiseuille flows in two-dimensional straight channels.
- The Nusselt number of favorable-pressure-gradient mixed flow is less than that of pure electro-osmotic flow, but higher than that of Poiseuille flow.

- For a particular source term, the Nusselt Number in adverse-pressure-driven mixed flow is higher than that of pure electro-osmotic flow.

Acknowledgments

The authors would like to acknowledge Dr. Hong-Ming Yin for his valuable suggestions. This work was funded by Washington State University Office of Research and Washington Technology Center.

References

1. J.P. Kutter, Current developments in electrophoretic and chromatographic separation methods on microfabricated devices. *Trac-Trends in Analyt. Chem.* 19 (2000) 352–363.
2. J. Yang, C.W. Li and M.S. Yang, Lab-on-a-chip (microfluidics) technology. *Acta Bioch. Biop. Sin.* 34 (2002) 117–123.
3. E. Verpoorte, Microfluidic chips for clinical and forensic analysis. *Electrophoresis* 23 (2002) 677–712.
4. H. Cui, H. Keisuke, P. Dutta and C.F. Ivory, Isoelectric focusing in a poly(dimethylsiloxane) microfluidic chip. *Analyt. Chem.* 77 (2005) 1303–1309.
5. P. Selvaganapathy, Y.S.L. Ki, P. Renaud and C.H. Mastrangelo, Bubble-free electrokinetic pumping. *J. Microelectromech. Syst.* 11 (2002) 448–453.
6. R.F. Probstein, *Physiochemical Hydrodynamics*. Second ed. New York: Wiley and Sons (1994) 400 pp.
7. C.H. Chen and J.G. Santiago, A planar electro-osmotic micropump. *J. Microelectromech. Syst.* 11 (2002) 672–683.
8. J.A. Tripp, F. Svec, J.M.J. Fechet, S.L. Zeng, J.C. Mikkelsen and J.G. Santiago, High-pressure electro-osmotic pumps based on porous polymer monoliths. *Sensors Actuat. B* 99 (2004) 66–73.
9. Z. Fan and D.J. Harrison, Micromachining of capillary electrophoresis injectors and separators on glass chips and evaluation of flow at capillary intersections. *Analyt. Chem.* 66 (1994) 177–184.
10. S.V. Ermakov, S.C. Jacobson and J.M. Ramsey, Computer simulations of electrokinetic transport in microfabricated channel structures. *Analyt. Chem.* 70 (1998) 4494–4504.
11. S.C. Jacobson, C.T. Culbertson, J.E. Daler and J.M. Ramsey, Microchip structures for submillisecond electrophoresis. *Analyt. Chem.* 70 (1998) 3476–3480.
12. K. Swinney and D.J. Bornhop, Quantification and evaluation of Joule heating in on-chip capillary electrophoresis. *Electrophoresis* 23 (2002) 613–620.
13. D.S. Burgi, K. Salomon and R.L. Chien, Methods for calculating the internal temperature of capillary columns during capillary electrophoresis. *J. Liq. Chromatogr.* 14 (1991) 847–867.
14. D. Maynes and B.W. Webb, Fully developed electro-osmotic heat transfer in microchannels. *Int. J. Heat Mass Transfer* 46 (2003) 1359–1369.
15. D. Maynes and B.W. Webb, Fully-developed thermal transport in combined pressure and electro-osmotically driven flow in microchannels. *J. Heat Transfer Trans. ASME* 125 (2003) 889–895.
16. D. Ross and L.E. Locascio, Microfluidic temperature gradient focusing. *Analyt. Chem.* 74 (2002) 2556–2564.
17. L. Graetz, Ueber die Wärmeleitungsfähigkeit von Flüssigkeiten (Erste Abhandlumg). *Ann. Phys. Chem.* 18 (1883) 78–94.
18. H.C. Agrawal, Heat transfer in laminar flow between parallel plates at small Peclet numbers. *Appl. Sci. Res.* A9 (1960) 177–189.
19. C.J. Hsu, An exact analysis of low Peclet number thermal entry region heat transfer in transversally nonuniform velocity fields. *AIChE J.* 17 (1971) 732–740.
20. M.L. Michelsen and J. Villadsen, The Graetz problem with axial heat conduction. *Int. J. Heat Mass Transfer* 17 (1974) 1391–1402.
21. E. Papoutsakis, D. Ramkrishna and H.C. Lim, The extended Graetz problem with prescribed wall flux. *AIChE J.* 26 (1980) 779–787.
22. J. Lahjomri and A. Oubarra, Analytical solution of the Graetz problem with axial conduction. *J. Heat Transfer Trans. ASME* 121 (1999) 1078–1083.
23. A.S. Telles, E.M. Querioz and G.E. Filho, Solution of the extended Graetz problem. *Int. J. Heat Mass Transfer* 44 (2001) 471–483.

24. B. Weigand, M. Kanzamar and H. Beer, The extended Graetz problem with piecewise constant wall heat flux for pipe and channel flows. *Int. J. Heat Mass Transfer* 44 (2001) 3941–3952.
25. J. Lahjomri, K. Zniber, A. Oubarra and A. Alemany, Heat transfer by laminar Hartmann's flow in thermal entrance region with uniform wall heat flux: the Graetz problem extended. *Energy Conv. Manag.* 44 (2003) 11–34.
26. E.M. Sparrow, J.L. Novotny and S.H. Lin, Laminar flow of a heat-generating fluid in a parallel-plate channel. *AIChE J.* 9 (1963) 797–804.
27. K. Horiuchi and P. Dutta, Joule heating effects in electroosmotically driven microchannel flows. *Int. J. Heat Mass Transfer* 47 (2004) 3085–3095.
28. P. Dutta and A. Beskok, Analytical solution of combined electroosmotic/pressure driven flows in two-dimensional straight channels: finite debye layer effects. *Analyt. Chem.* 73 (2001) 1979–1986.
29. J. Lyklema, S. Rovillard and J. De Coninck, Electrokinetics: the properties of the stagnant layer unraveled. *ACS J. Surf. Colloids* 14 (1998) 5659–5663.
30. G. Arfken, *Mathematical Methods for Physicists. Third ed.* Boca Raton, FL: Academic Press (1985) 815 pp.
31. L.C. Burmeister, *Convective Heat Transfer*. New York: Wiley and Sons (1994) 790 pp.
32. R.D. Cess and E.C. Shaffer, Heat transfer to laminar flow between parallel plates with a prescribed wall heat flux. *Appl. Sci. Res.* A8 (1959) 339–344.